Improving the thermal-hydraulic performance of parabolic solar collectors using absorber tubes equipped with perforated twisted tape containing nanofluid

Awatef Abidi [a,b,c,*], A.S. El-Shafay [d], Mohamed Degani [e,f], Kamel Guedri [g,h], S. Mohammad Sajadi [i,j], Mohsen Sharifpur [k,l,*]

[a] Physics Department, College of Sciences Abha, King Khalid University, Saudi Arabia
[b] Research Laboratory of Metrology and Energy Systems, National Engineering School, Energy Engineering Department, Monastir University, Monastir City, Tunisia
[c] Higher School of Sciences and Technology of Hammam Sousse, Sousse University, Tunisia
[d] Department of Mechanical Engineering, College of Engineering, Prince Sattam bin Abdulaziz University, Alkharj 16273, Saudi Arabia
[e] Mechanical Engineering Department, College of Engineering, Jazan University, Saudi Arabia
[f] Higher Institute of Technological Studies of Sousse, Tunisia
[g] Mechanical Engineering Department, College of Engineering and Islamic Architecture, Umm Al-Qura University, B. Po 5555, Makkah 21955, Saudi Arabia
[h] UR: « Matériaux, Energie et Energies Renouvelables » (MEER), Faculty of Sciences of Gafsa, B.P.19-2112 Zarroug, Gafsa 2100, Tunisia
[i] Department of Nutrition, Cihan University-Erbil, Kurdistan Region, Iraq
[j] Department of Phytochemistry, SRC, Soran University, KRG, Iraq
[k] Department of Mechanical and Aeronautical Engineering, University of Pretoria, South Africa
[l] Department of Medical Research, China Medical University Hospital, China Medical University, Taichung, Taiwan

ARTICLE INFO

Keywords:
Solar collector
Perforated twisted tape
Nanofluid
Energy and exergy efficiencies

ABSTRACT

The thermal and hydraulic efficiency of a parabolic trough solar collector is investigated in this study. The collector absorber tube is equipped with twisted tape with circular holes containing water-copper oxide nanofluid with three nanoparticles volume fractions of 1%, 2% and 4%. In three modes (d/W = 0.5, 0.7, 0.9), circular holes are constructed for the ratio of the circle's diameter to the twisted tape's breadth. All turbulent flow simulations were done using the SIMPLEC algorithm, FVM and RNG k-ε model in three Reynolds numbers as 10,000, 20,000 and 30,000. Studies have shown inserting twisted tape with a circular hole increases the pressure drop and the heat transfer rate compared to a pipe without twisted tape. The highest coefficient of thermal performance occurs in Reylond number of 10,000 and a nanoparticles volume fraction of 4%. The findings indicate that using nanoparticles improves the solar collector's energy and exergy efficiency. As a result, the best collector performance was obtained when using nanofluids with an nanoparticles volume fraction of 4%.

Introduction

The intensification in the world population has led to the rise in global energy demand. Fossil fuels, nuclear power, and renewable energy are the primary sources of energy today [1–4]. Currently, fossil fuels and nuclear energy are covering 91% of world energy demand, whereas renewable energy resources cover only 9%.

Therefore, different researchers have sought to reduce energy consumption by humans by expressing different solutions [5–9]. In addition, some of them have attempted to improve the efficiency of various gadgets by using techniques such as nanofluids (NFs), different types of blades, magnetic field, etc. [10–16]. Other researchers, however, have sought to find new sources of energy and improve their efficiency [17–19].

Solar energy [20,21] help solve global energy crises, save costs and reduce bills because solar energy is renewable and clean energy source that is the most abundant, inexhaustible, universal source of energy, the most accessible, free, cost-effective, and as a pollution less, sustainable source of energy [22–26].

Among the solar collectors (SCs) types, parabolic trough solar

* Corresponding authors at: Physics Department, College of Sciences Abha, King Khalid University, Saudi Arabia (A. Abidi). Department of Mechanical and Aeronautical Engineering, University of Pretoria, South Africa (M. Sharifpur).
E-mail addresses: abidiawatef@yahoo.fr (A. Abidi), mohsen.sharifpur@up.ac.za (M. Sharifpur).

Table 1
Recent studies in PTC absorber.

Year	Authors	Type Inserts	Method	Receiver Material, HTF, Boundary condition	Result	Model
2013	Mwesigye et al. [40]	Twisted tape that is attached to the wall	CFD	Stainless steel/Syltherm 800 uniform heat flux Re = 10,260 to 320,000	• Nu was 1.01–3.36 times • Friction factor was 1.32–21.8 times • Thermal enhancement factor was 0.74–1.25 times	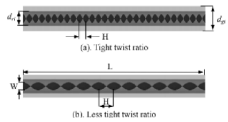
2014	Zamzamian et al. [41]	Louvered twisted tape	CFD	Aisi304/Aluminum/ Behran Thermal Oil Non-uniform heat flux Re = 5000	• Nu rises up to 150% • Friction factor rises up to 210%	
2014	Song et al. [42] _reference	Screw tape with helical axis	CFD	Dowtherm-A Non-uniform heat flux	• Heat loss reduced by 6 times • Friction factor augmented 23 times • Pressure loss increases 4 times	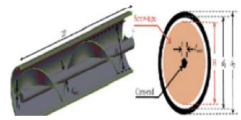
2015	Changa et al. [43]	Twisted tape	CFD	Heat flux was non-uniform Molten Salt/Nickel-Chromium Alloy Re = 10,200 to 1,360,000	• Nu boosts your performance by around 2.9 times. • The friction factor increases by 2.5 times.	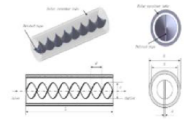
2016	Mwesigye et al. [44]	Wall-detached twisted tape	CFD	Stainless Steel/Syltherm 800 Non-uniform heat flux Re = 10,300 – 1,360,000	• HTR performance was about 69% • Thermal efficiency enhanced in the range of 5%–10% • Entropy generation diminished up to 58.8%. • The HTC enhanced from 1.05 to 2.69 • Friction factor augmented from 1.6 to 14.5	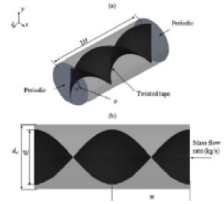
2016	Liu et al. [45]	Two twisted tape	CFD	Water/steam	• In the receiver, longitudinal vortexes generated alongside the main flow efficiently reduce the peripheral temperature differential from 69 K to 42 K.	
2016	Jaramillo et al. [46]	Twisted tape	CFD	Copper tube/Aluminum Strip/Water	• Achieving the set of circumstances under which a twisted tape insert may be used to boost a PTSC's efficiency.	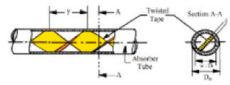
2017	Zhu et al. [47]	Wavy-tape	CFD	Syltherm-800 Non uniform heat flux	• Nu increased in the range of 261–310% • Heat diminished in the range of 17.5–33.1% • Friction factor augmented in the range of 382–405%. • Total entropy generation rate decreased in the range of 30.2–81.8%	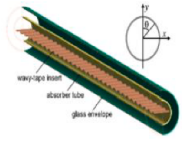
2017	Rawani et al. [48]	Serrated twisted tape Serrated twisted tape and metal foam	CFD	Therminol-VP1	• Thermal efficiency increased 3% and 5% using metal foam and serrated twisted tape, respectively.	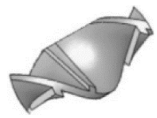
2019	Liu et al. [49]	Inclined conical strip	CFD	Stainless steel/Syltherm-800 uniform heat flux Re = 5000 to 791,000	• The most significant reduction in entropy production was 74.2 percent. • The 82.1 percent decrease in heat loss is the highest. • The highest increase in exergetic efficiency was about 5.7 percent. • Thermal efficiency improved by 0.02–5.04%	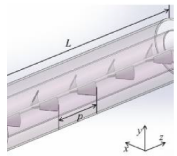
2020	Amani et al. [50]	Conical strip	CFD	Re = 8000 to 40,000.	• Nu intensifies up to 91.949%. • The friction factor was 5.21 times higher than the standard PTC. • PEC varied from 1.107 to 0.679.	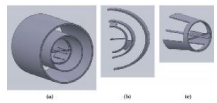
2020	Suresh et al. [51]	Modified twisted tapes	exp	copper absorber tube	• Nu increased in the range of 5–40% by typical twisted tape. • Nu enhanced in the range of 11–101% using twisted tape with attached rings. • Twisted tapes with modified connected rings enhanced Nu in the range of 7–77 percent.	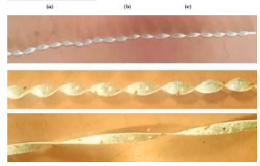

(*continued on next page*)

Table 1 (*continued*)

Year	Authors	Type Inserts	Method	Receiver Material, HTF, Boundary condition	Result	Model
2021	Xiao et al. [52]	Baffles with a curved, twisted shape	CFD	Syltherm 800 Non-uniform heat flux	• Overall efficiency enhanced 0.52% • Exergy efficiency increased 0.22%	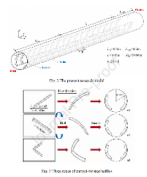
2021	Vasanthi and Jaya Chandra reddy [53]	twisted strip with an angular shape	Exp	Stainless steel copper tube/water	• Efficiency enhanced in the range of 145–215%.	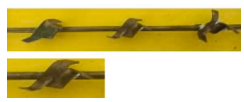
2015	Diwan and Soni [54]	Wire coil	CFD	Water Uniform heat flux	• Nusselt number increased 104% to 330%	
2015	Sahin et al. [55]	Wire coil	CFD + EXP	Water	• Turbulators improve heat transmission up to 2.28, 2.07, and 1.95 times better than a smooth tube.	
2020	Yılmaz et al. [56]	Wire coil	CFD	Therminol®VP-1 steel absorber tube	• HTR Performance increased 183%. • thermal efficiency improvement was 0.4%.	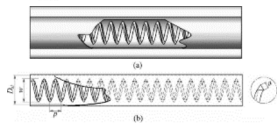

collectors (PTSCs) are commercially efficient, cost-effective, and technically the most advanced technology for concentrated solar energy with a concentration ratio of 10 to 50 [27–30]. These collectors can work by thermal oil and molten salts in temperatures up to 400 °C and 550° C, respectively. They can be used for a variety of industrial and domestic applications.

PTSCs are a type of heat exchanger in which methods of augmenting heat transfer rate (HTR) for common types of heat exchangers can be used in these systems. Increasing the heat transfer coefficient (HTC) between the absorber pipe and the heat transfer fluid to increase the HTR, increase thermal efficiency, and lower the temperature variation surrounding the adsorbent pipe to reduce thermal stresses and, therefore, reduce the risk of failure. Previous studies are presented in Table 1 for a better and easier review and the possibility of comparing related studies in the field of PTSCs. Applying nanoparticles is of paramount importance to improve heat transfer [31–37]. Regarding this, Bahrami et al. [38] used water/Al_2O_3 to boost forced convection heat transfer due to the higher thermal conductivity of particles. Nguyen et al. [39] reported that carbon nanotube particles are decisive factors in augmenting the efficiency of a heat exchanger.

According to previous studies, the need to improve the efficiency of solar collectors using passive methods is absolutely essential. In this study, the aim is to increase the solar collector's efficiency and thermal-hydraulic behavior by using twisted tape. To reduce the negative effect of twisted tape application on increasing pressure drop, holes have been used in the geometry of twisted tape to achieve the highest PEC value.

Based on the review of previous studies, the efficiency and thermal-hydraulic performance of PTSCs with perforated twisted tapes in the absorber tube are investigated in the present paper for different Re, various nanoparticles volume fraction (NVFs), and different sizes of holes on the twisted tapes.

Geometric model

Using numerical methods are studied in various studies [57–63]. In the present study, an absorber tube possessing a twisted tape with perforated twisted tapes is used to improve the HTR and efficiency of the SC. Circular holes are designed for different ratios of the hole's diameter to the width of the twisted tape, d/W = 0.5, 0.7, and 0.9. In these models, the twisted ratio y/W is 3 and the thickness of the twisted tape is 1 mm. The geometry specifications are shown in Table 2, and the shape of the perforated twisted tape is shown in Fig. 1.Figs. 2 and 3

Effect of NF

Conventional fluids used for heat transfer have a low thermal conductivity [64–68]. According to experimental findings, the thermal conductivity of the NF is substantially improved when nanoparticles are added to the water. As a result, NFs are ideal for use in heat transfer applications. Because nanoparticles have high conductivity, their suspension in a base fluid increases its thermal conductivity, which is one of the most important factors in heat transfer. These particles are made of metal such as copper, silver, etc., or metal oxides such as aluminum oxide, copper oxide, etc. In this study, copper oxide (CuO) particles with different NVFs are added to the base fluid, i.e. water, to boost HTR. The NF's characteristics are presented in Table 3.

Mathematical & numerical methodology

Governing equations

The fluid is assumed to be Newtonian and incompressible to simplify the numerical calculations. Consequently, the flow is steady, and the

Table 2
The performed dimensions parameters.

Parameter	Amount
Re	1000–2000-3000
Twisted ratio	3
Inner tube diameter (D)	22 mm
Twisted tape width (W)	20 mm
Twisting length (y)	60 mm
Twisted tape length (y)	600 mm
Twisted tape thickness (t)	1 mm

effects of gravity are negligible. Governing equations, i.e. continuity, momentum, and energy, are as follows, respectively:

$$\frac{\partial}{\partial x_i}(\rho u_i) = 0 \tag{1}$$

$$\frac{\partial}{\partial x_j}(\rho u_i u_i) = -\frac{\partial p}{\partial x_i} + \frac{\partial}{\partial x_j}\left[\mu\left(\frac{\partial u_i}{\partial x_j} + \frac{\partial u_j}{\partial x_i}\right) - \rho\overline{u_i' u_j'}\right] \tag{2}$$

$$\frac{\partial}{\partial xj}(\rho u T) = \frac{\partial}{\partial xj}\left((\Gamma + \Gamma_t)\frac{\partial T}{\partial x_j}\right) \tag{3}$$

where u, ρ, and μ are the velocity, the fluid density, and the dynamic viscosity, respectively.

Simulations are performed for heat transfer analysis include Reynolds number (Re), Nusselt number (Nu), coefficient of friction (f), Performance Evaluation Criteria (PEC), and collector energy and exergy efficiency.

$$Re = \frac{\rho u D}{\mu} \tag{4}$$

$$Nu = \frac{hD}{k} \tag{5}$$

where the thermal conductivity for the working fluid is k.

The friction coefficient in turbulent flow inside the pipe is determined using the following equation:

$$f = \frac{2\Delta P D}{\rho L u^2} \tag{6}$$

The PEC is a parameter utilized to assess the thermal behavior of a fluid flow in a heat exchanger or SC. This coefficient is described for the (Nu/Nu_p) to (f/f_p) under the same conditions [30].

$$PEC = (Nu/Nu_p)/(f/f_p)^{1/3} \tag{7}$$

where Nu_p is pipe Nusselt number and Nu is the Nusselt number for pipe equipped with a perforated twisted tape. f_p is pipe friction coefficient and f is the friction coefficient of the pipe equipped with a perforated twisted tape.

The thermal performance of SCs is analyzed using thermal efficiency.

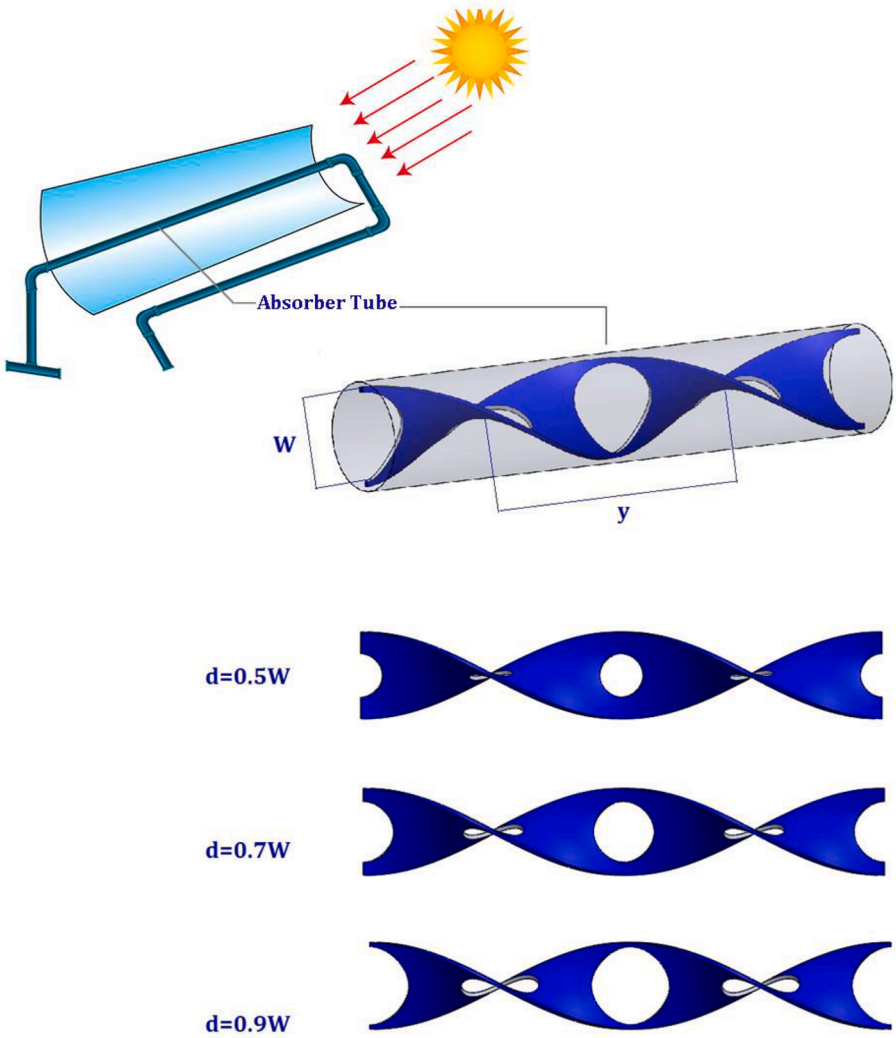

Fig. 1. SC with three perforated twisted tapes of various diameters in the absorber tube.

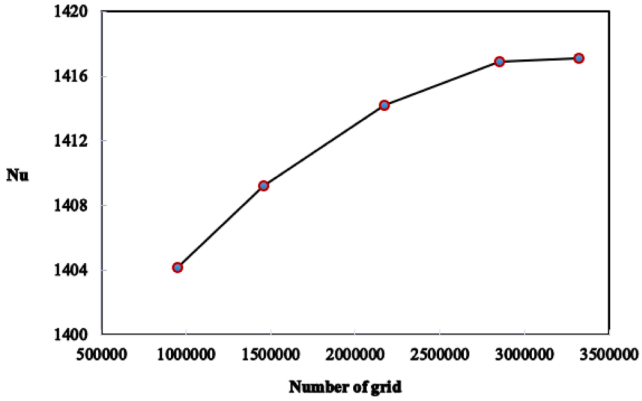

Fig. 2. Grid independence.

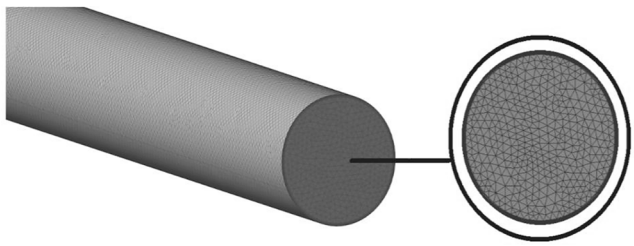

Fig. 3. View of the absorber tube grid.

Table 3
Characteristics of NFs with copper oxide particles for three different NVFs.

NF	$\rho(kg.m^{-3})$	$\mu(kg.m^{-1}.s^{-1})$	$k(W.m^{-1}.K^{-1})$	$C_p(J.kg^{-1}.K^{-1})$
water + 1%*CuO*	1050.33	0.001080	0.631	3959.7
water + 2%*CuO*	1103.56	0.001198	0.650	3761.7
water + 4%*CuO*	1210.02	0.001493	0.680	3581.8

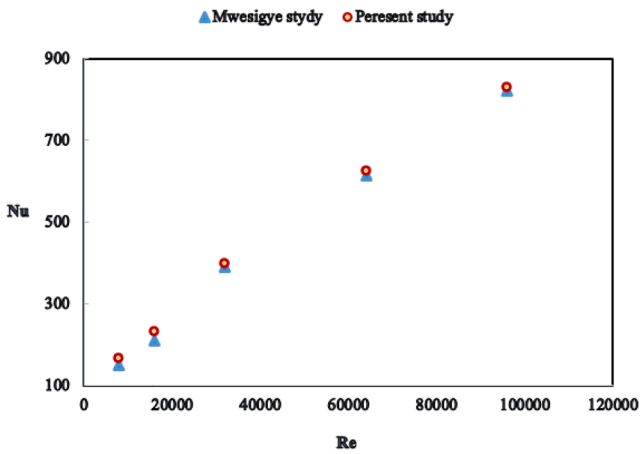

Fig. 4. Nu for the present study compared with Mwesigye et al. [44].

Thermal efficiency is described as the ratio of the energy absorbed by the fluid flowing in the absorber tube to the direct radiative energy received by the surface of the reflector plate.

$$\eta_c = \frac{Q_{in}\rho_{in}c_{Pin}(T_{out} - T_{in})}{6 \times 10^4 IA} \tag{8}$$

Exergy efficiency or second-law efficiency of PTSCs is expressed as

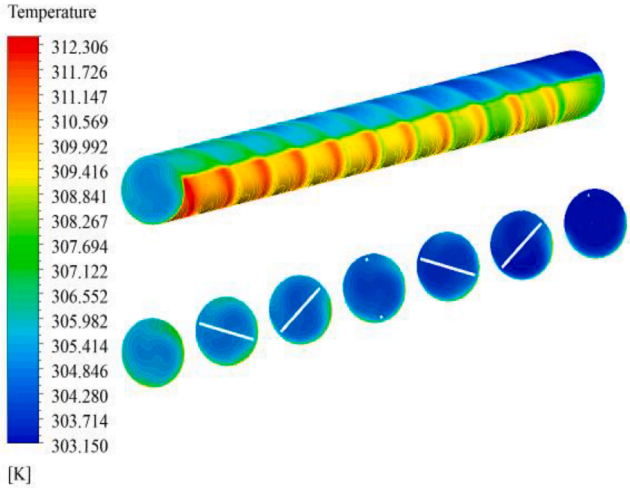

Fig. 5. Temperature field inside the absorber tube and the plates with different distances.

net beneficial exergy divided by the exergy of solar irradiance entering the collector:

$$\eta_{ex} = \frac{\dot{Q}_{HTF} - \dot{m}_{HTF}C_{P,HTF}\ln\left(\frac{T_\infty}{T_{i,HTF}}\right)}{\dot{Q}_{HTF} - \dot{m}_{BF}C_{P,BF}\ln\left(\frac{T_{o,BF}}{T_{i,BF}}\right) + VI\eta_P} \tag{9}$$

where η_P is the pump efficiency that is considered equal to 85%.

Numerical method

As many studies have shown, numerical techniques are one of the most cost-effective ways to analyze the efficiency of a wide range of applicants [69,70]. Therefore, this paper performs the simulations using ANSYS FLUENT software version 2020. The k-ε turbulence model is utilized modeling the turbulent flow. This model is a common two-equation turbulence model that includes two transport equations to calculate the turbulent flow properties. These equations can be used to calculate the effects of advection and diffusion on turbulent energy. In this model, the turbulent field is expressed in terms of the two variables of turbulent kinetic energy (k) and turbulence energy dissipation rate (ε). In other words, k determines the turbulent energy, and ε determines the magnitude of turbulence. The k-ε model is implemented in FLUENT software in three different approaches. The general form of transport equations for k and ε is the same in these models. The difference between them is in the methods of calculating the turbulent viscosity, the turbulent Prandtl number governing the turbulence distribution k and ε, and the additional components in the ε equation. In this study, the RNG model is employed, which has higher accuracy than the other ones. To couple pressure and velocity fields, the SIMPLEC algorithm is used. The governing equations are first solved on a grid with an optimal number of nodes using a first-order forward discretization scheme for numerical solution convergence. The under relaxation factors are also applied so that the solution reaches convergence faster. After the initial convergence, the under relaxation factors increase, and finally, the second-order discretization scheme is used. The convergence criterion of the numerical solution is 10^{-6} for all variables. In calculating the properties (viscosity and thermal conductivity), due to the lack of large changes in temperature, only relationships dependent on the volume fraction have been used. Properties for different volume fractions are calculated and presented in Table 3. Also, due to the fact that the volume fraction of nanoparticles in nanofluids is not high, the single phase model has been used to simulate nanofluids.

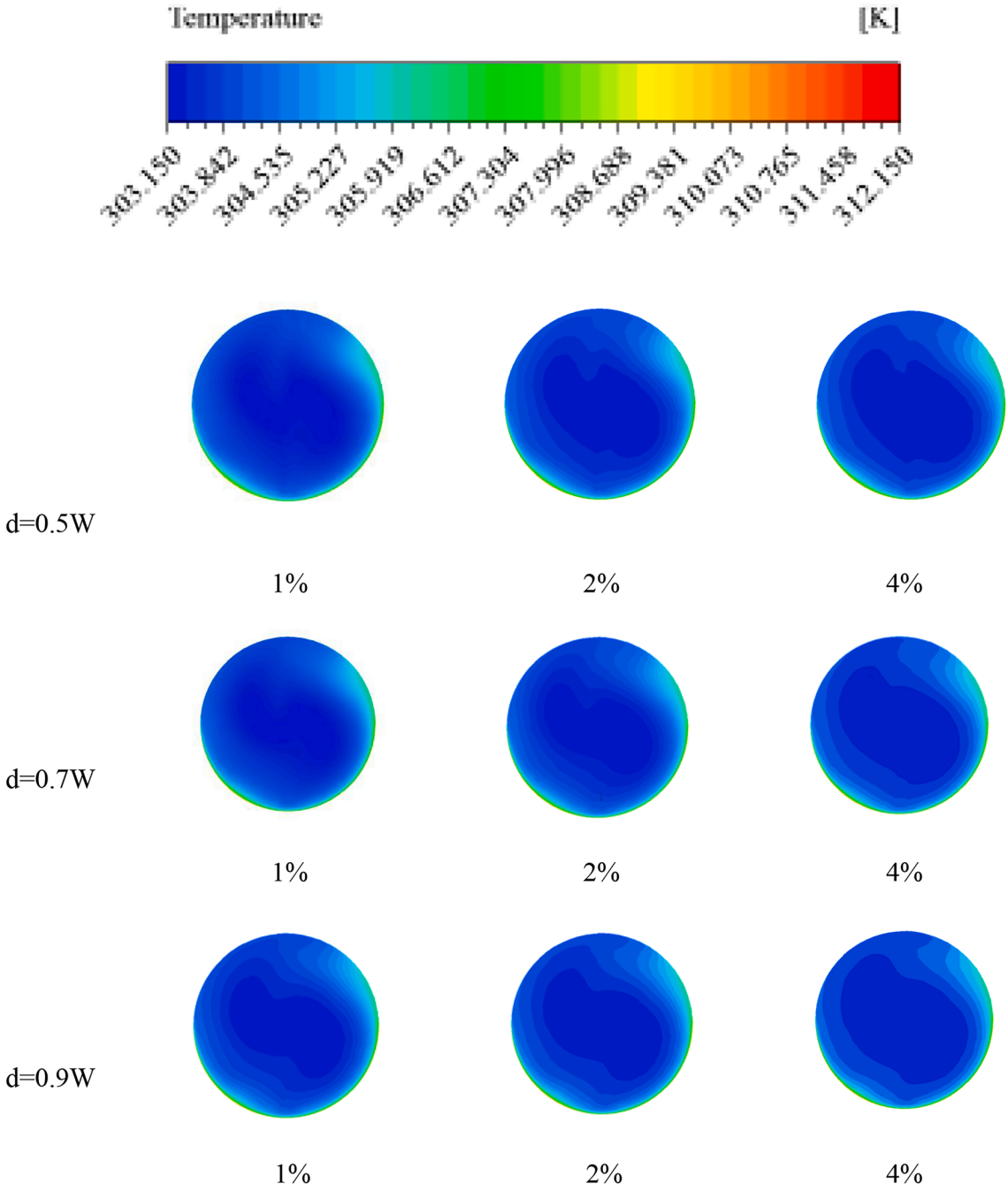

Fig. 6. Temperature field of the tube with a perforated twisted tape and NF with different NVFs when Re is 10,000 at the outlet.

Boundary conditions

The following are the boundary conditions that are applied to the absorber tube with perforated twisted tapes for numerical solution:

Inlet boundary condition

The fluid flow has a uniform u and T which enter the tube are:
$u = u^{\circ}$, $T = T = 30^{\circ}C$
Wall
The flux in the upper half wall and lower half wall of the pipe is obtained using the following equation:

$q_{up} = I_g$

$q_{down} = I_b C_R$

where I_g is the total radiation that is the same as 700 W/m^2, I_b is direct radiation that is the same as 650 W/m^{2,} and C_R is assumed to be 30.

Outlet

The zero pressure is used at the end of the geometry.

Grid independence test

The computational domain is meshed using ANSYS Mashing 2020 software. The grid cells are quadrilateral type generated using the bottom-up algorithm so that the grid is finer close to the perforated

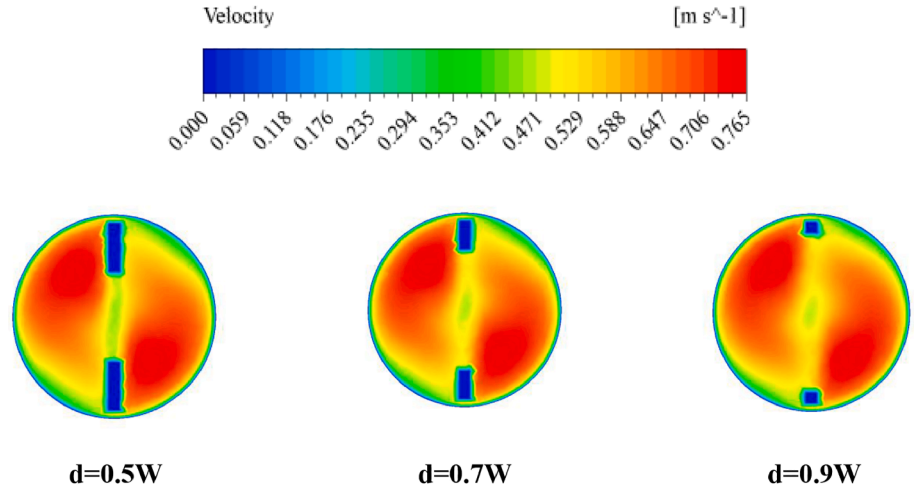

Fig. 7. Velocity contours at the outlet for a NVF = 4% at Re of 10000.

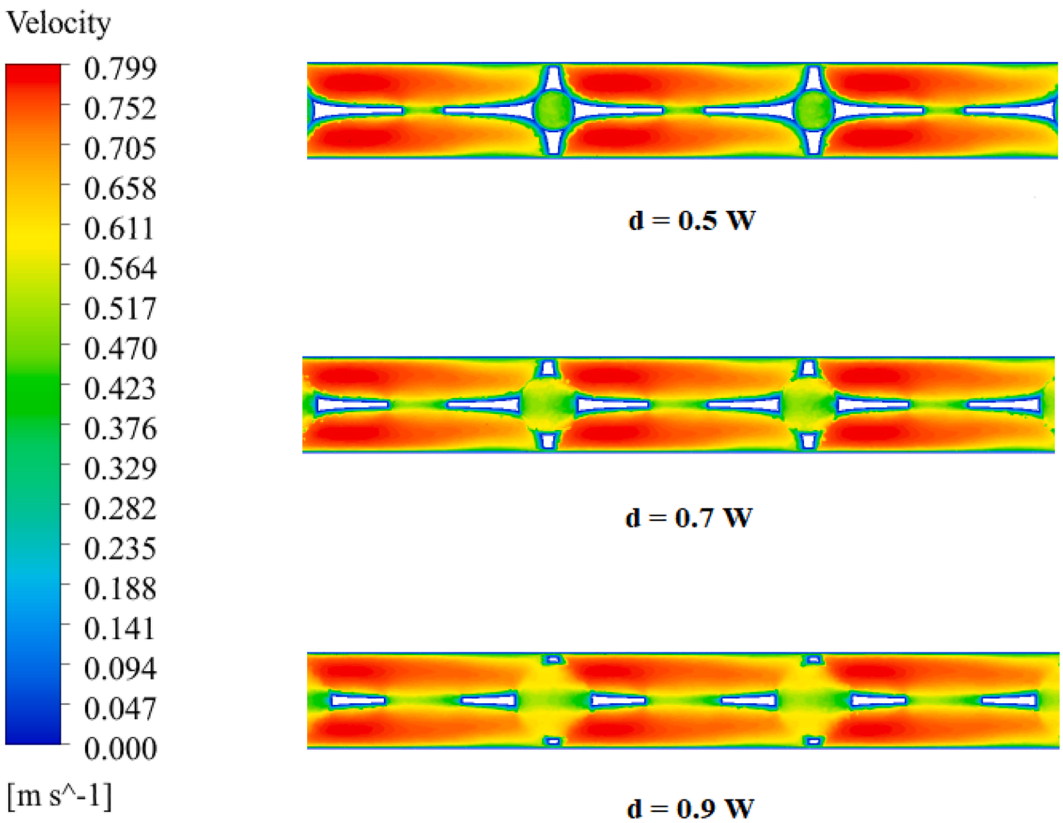

Fig. 8. Velocity contours at the middle plane of the tube for a NVF = 4% at Re of 10000.

twisted tape. Also, a boundary layer mesh is used in close proximity to the tube wall. In addition to creating logical and acceptable results, the grid must also be computational cost-effective. The simulations are performed for five grids with 950200, 1486900, 2173500, 2852300, and 3,323,500 elements. Since no noticeable changes are observed in the results, the grid with 2,852,300 elements is selected as the main grid to reduce the computational cost.

Validation

To guarantee that numerical findings are accurate, the ahead numerical results must be validated with numerical or experimental results. To assess the accuracy of the current numerical work, first, the simulated outcomes of Mwesigye et al.[44], who investigated the HTR in the absorber tube of a PTSC with a classically twisted tape, is viewed. According to Mwesigye et al. [44] research, an absorber tube with a twisted tape with dimensional parameters and boundary conditions is

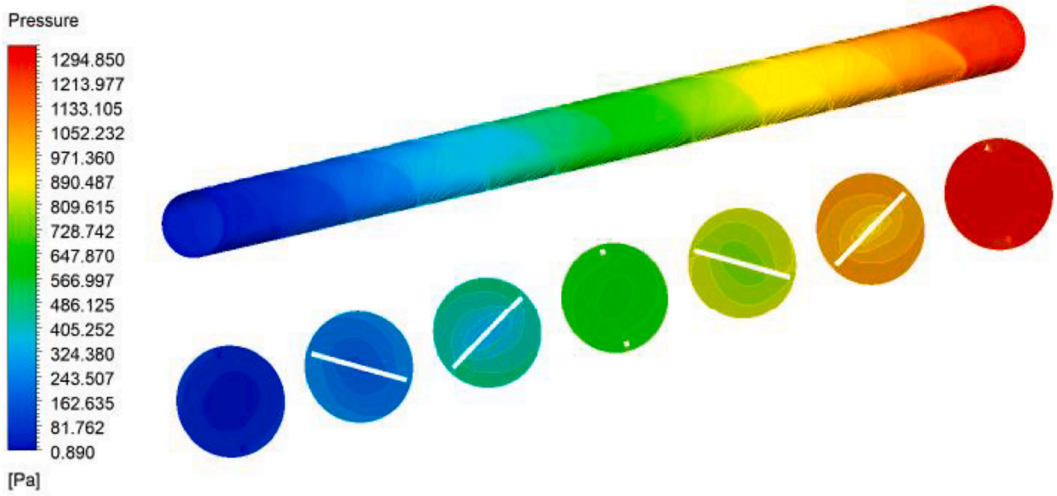

Fig. 9. Pressure changes along the tube supplied with a perforated twisted tape for d = 0.9 W and a NVF = 4% at Re of 10000.

simulated and evaluated. The Nu findings for various Re values are given in Fig. 4. As can be seen, the Nu in the present simulations agrees with Mwesigye et al. [44], so the accuracy of the modeling results in the present study is ensured.

Analysis of numerical results

The numerical results produced from the current simulations are used to assess effective parameters in this section, including Nu, f, PEC, and energy and exergy efficiency of a PTSC with a tube with a perforated twisted tape in the presence of NF containing CuO particles with different NVFs. In addition, the results are evaluated for three Re of 10,000, 20,000, and 30,000 to determine the best optimal geometry.

Fig. 5 depicts the temperature field contours inside the absorber tube and the plates with different distances. According to the governing boundary conditions, the maximum temperature enhancement occurs at the bottom of the tube due to the maximum heat flux. After that, the temperature gradually enhances as it approaches the tube outlet.

Fig. 6 demonstrates the temperature contours at the tube outlet for a twisted tape with three different circular holes for different NVFs when the Re is 10,000. In all three models, HTR increases with the NVFs from 1 to 4%, and consequently, more temperature changes are observed. The average outlet temperature is 305 K when the NVF is 4%. As can be seen in this figure, as the dimensions of the hole increase, the thermal penetration into the flow increases. Higher energy exchange causes this behavior due to easier molecular collisions in these areas.

Based on Fig. 7, the twisted tape causes flow inside the tube to be divided into two parts. In the first model, where d = 0.5 W, the two flow sections are completely separate. By enhancing the diameter of the circular holes on the twisted tape, the mixing of two flows on both sides of the tape increases. The flow separation has the linear mode for the first model and changes to the O-shape for the third model with a ratio of d = 0.9 W. It is expected that as the hole's diameter increases, the fluid faces fewer obstacles, and the separation effect decreases. In each section, a rotational flow is observed so that the velocity is maximum close to the twisted tape. Fig. 8 shows the effect of the perforated twisted tape on U in the plane passing through the center of tube.

Fig. 9 exhibits the pressure changes along the absorber tube supplied with a perforated twisted tape for d = 0.9 W and NVF = 4%. As can be seen, the pressure decreases as the flow approaches the tube outlet and finally reaches atmospheric pressure at the outlet, which is zero gauge pressure. The pressure drop in this model is equal to 1295 Pa.

For the tube provided with a perforated twisted tape with various hole sizes, the Nu is shown in Fig. 10. Based on this, the Nu goes up with the Re. Also, growth in the NVF improves the conduction heat transfer and thus intensifies the Nu. As the size of the holes increases, the average Nusselt number decreases. The enlargement of the holes in the turbulator body prevents further turbulence in the flow, thus reducing heat exchange and reducing the average Nusselt number.

The pressure drop is shown in Fig. 11 for three twisted tape models with NF with various NVFs. Suspension of nanoparticles in the base fluid brings about an increment in fluid viscosity, leading to an enhancement in NF pressure loss. Also, the larger the Re, the higher the NF velocity, which increases the pressure drop.

Fig. 12 shows the friction coefficient for different NVFs in the absorber tube supplied with a perforated twisted tape for d = 0.9 W at three Re of 10,000, 20,000, and 30,000. The friction coefficient and the velocity are inversely correlated. Therefore, the friction coefficient is reduced with the Re. Also, the friction coefficient is enhanced with the NVFs, as a result of raising the density and viscosity. As the volume fraction of nanoparticles increases, the flow pressure drop increases. Increasing the volume fraction of nanoparticles increases the viscosity resulting in shear stresses and higher pressure drop.

Higher values of PEC mean greater thermo-hydraulic efficiency. When d = 0.9 W, the tube with a perforated twisted tape had the best PEC, according to all of the tests. By enhancing the NVFs, the PEC is reduced. Also, an increment in the Re leads to a reduction in the PEC. According to Fig. 13, the maximum value of PEC takes place at Re of 10,000 and a NVF = 1%. The maximum value is equal to 1.6, which is 61% higher than the PEC of the absorber tube without a perforated twisted tape for the same working fluid.

The thermal efficiency of a SC characterized by Eq. (8) is the most crucial variable for evaluating a collector. When d = 0.9 W, Fig. 14 shows the changes in thermal efficiency for a SC with a tube equipped with a perforated twisted tape with NF at different NVFs. As can be seen, the thermal conductivity of the NF increases with the NVF, causing more absorption of solar radiation and thus an increase in the generation of thermal energy. The NF with a NVF = 4% has a maximum thermal

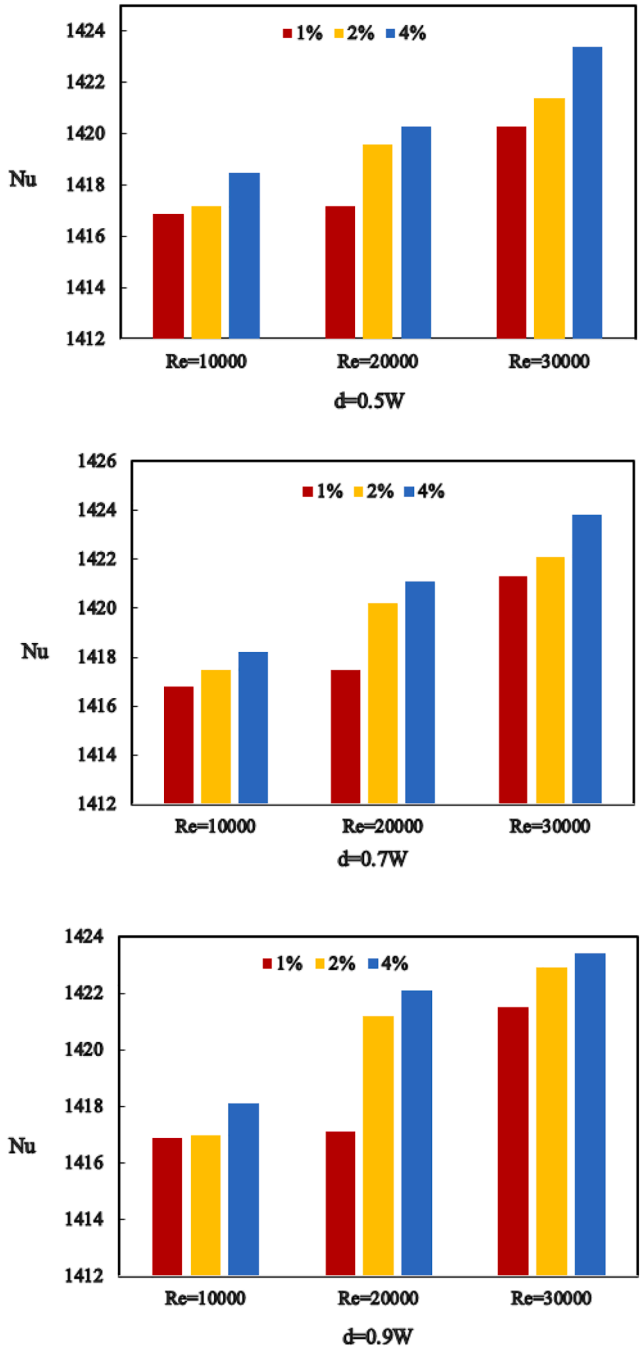

Fig. 10. The quantity of Nu in the tube provided with a perforated twisted tape for three Re values of 10,000, 20,000, and 30,000 for various NVFs.

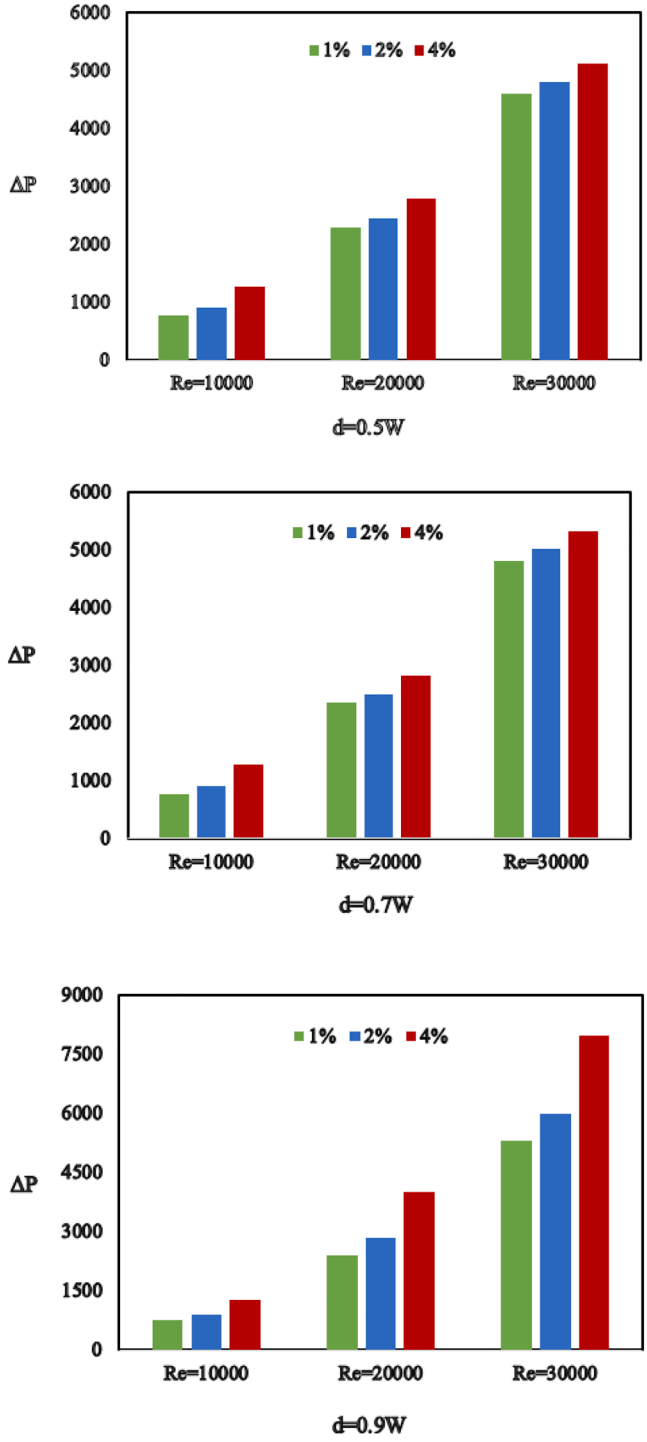

Fig. 11. The amount of pressure drop (kPa) inside the tube supplied with a perforated twisted tape for different NVFs at three Re of 10,000, 20,000, and 30,000.

efficiency of 64%. As the NVF is enhanced, the mass flow rate goes up, and the velocity is reduced. Therefore, according to Eq. (9), enhancing the concentration of working fluid augments the exergy efficiency of the collector. The NF with NVF = 4% has the maximum exergy efficiency of 28%.

Conclusions

The present study evaluates a tube supplied with a perforated twisted tape with varying proportions of the hole's diameter to the width of the twisted tape, d/W = 0.5, 0.7, and 0.9 in the presence of water-CuO NF with different NVFs)Re 10,000, 20,000 and 30,000(.

- The use of NF enhances the HTR and pressure loss in the tube so that the higher the concentration of nanofluid, the higher the amount of Nu and pressure drop.
- Exerting perforated twisted tape enhances the HTR (Nusselt number) compared to a tube without a tape. As the diameter of the circular hole increases, the flow is mixed across both sides of the twisted tape, and the pressure drop is reduced.

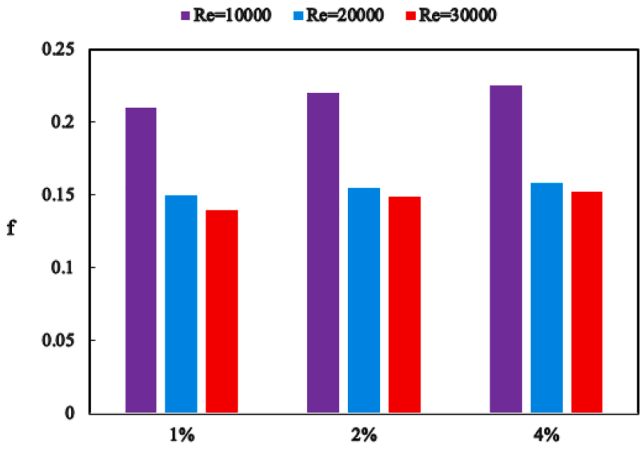

Fig. 12. The amount of friction coefficient inside the tube supplied with a perforated twisted tape for d = 0.9 W, various NVFs, and three Re of 10,000, 20,000, and 30,000.

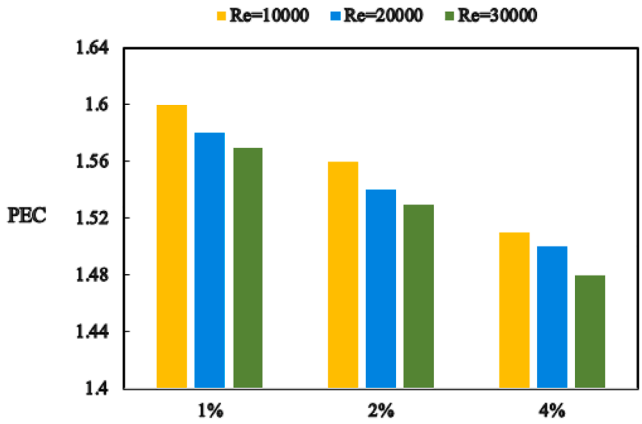

Fig. 13. The amount of PEC for the tube supplied with a perforated twisted tape for d = 0.9 W, different NVFs, and three Re of 10,000, 20,000, and 30,000.

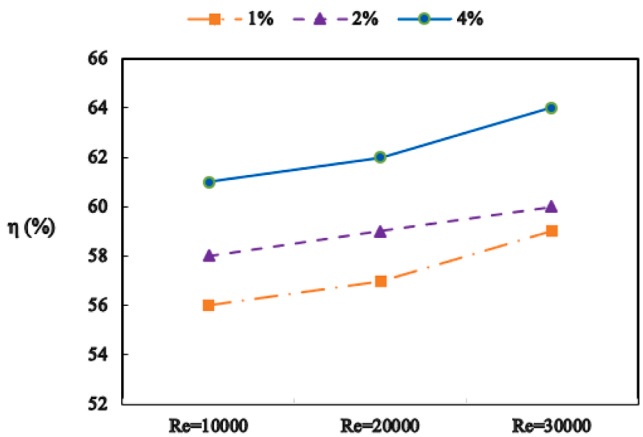

Fig. 14. SC efficiency regarding Re for the NF with different NVFs.

- The maximum PEC occurs at Re of 10,000 and a NVF = 4%.
- The best performance for NF is achieved for the NVF = 4%.
- For NF, the highest exergy efficiency is attained with NVF = 4%, which is equal to 28%.

Declaration of Competing Interest

The authors declare that they have no known competing financial interests or personal relationships that could have appeared to influence the work reported in this paper.

Acknowledgments

The authors extend their appreciation to the Deanship of Scientific Research at King Khalid University, Abha, Saudi Arabia for funding this work through the Research Group under grant number (R.G.P.2/55/43)

References

[1] Chan H-Y, Riffat SB, Zhu J. Review of passive solar heating and cooling technologies. Renew Sustain Energy Rev 2010;14(2):781–9.
[2] Rahmani E, Moradi T, Fattahi A, Delpisheh M, Karimi N, Ommi F, et al. Numerical simulation of a solar air heater equipped with wavy and raccoon-shaped fins: The effect of fins' height. Sustainable Energy Technol Assess 2021;45:101227. https://doi.org/10.1016/j.seta.2021.101227.
[3] Habib R, Yadollahi B, Saeed A, Doranehgard MH, Karimi N. On the Response of Ultralean Combustion of CH4/H2 Blends in a Porous Burner to Fluctuations in Fuel Flow—an Experimental Investigation. Energy Fuels 2021;35(10):8909–21.
[4] Wang HUANKUN, Leaney PG. Modelling and energy efficiency analysis of a hybrid pump-controlled asymmetric (single-rod) cylinder drive system. International Journal of Hydromechatronics 2020;3(1):1. https://doi.org/10.1504/IJHM.2020.10026989.
[5] Hajatzadeh Pordanjani A, Aghakhani S, Afrand M, Mahmoudi B, Mahian O, Wongwises S. An updated review on application of nanofluids in heat exchangers for saving energy. Energy Convers Manage 2019;198:111886. https://doi.org/10.1016/j.enconman.2019.111886.
[6] Pordanjani AH, Aghakhani S, Afrand M, Sharifpur M, Meyer JP, Xu H, et al. Nanofluids: Physical phenomena, applications in thermal systems and the environment effects- a critical review. J Cleaner Prod 2021;128573.
[7] Sarsam WS, Kazi SN, Badarudin A. A review of studies on using nanofluids in flat-plate solar collectors. Sol Energy 2015;122:1245–65.
[8] Alizadeh R, Gomari SR, Alizadeh A, Karimi N, Li LKB. Combined heat and mass transfer and thermodynamic irreversibilities in the stagnation-point flow of Casson rheological fluid over a cylinder with catalytic reactions and inside a porous medium under local thermal nonequilibrium. Comput Math Appl 2021;81:786–810.
[9] Sadeghi MS, Dogonchi AS, Ghodrat M, Chamkha AJ, Alhumade H, Karimi N. Natural convection of CuO-water nanofluid in a conventional oil/water separator cavity: Application to combined-cycle power plants. J Taiwan Inst Chem Eng 2021.
[10] Yan S-R, Aghakhani S, Karimipour A. Influence of a membrane on nanofluid heat transfer and irreversibilities inside a cavity with two constant-temperature semicircular sources on the lower wall: applicable to solar collectors. Phys Scr 2020;95(8):085702. https://doi.org/10.1088/1402-4896/ab93e4.
[11] Pordanjani AH, Raisi A, Ghasemi B. Numerical simulation of the magnetic field and Joule heating effects on force convection flow through parallel-plate microchannel in the presence of viscous dissipation effect. Numerical Heat Transfer, Part A: Applications 2019:1–18.
[12] Pordanjani AH, Aghakhani S. Numerical Investigation of Natural Convection and Irreversibilities between Two Inclined Concentric Cylinders in Presence of Uniform Magnetic Field and Radiation. Heat Transfer Eng 2021:1–21.
[13] Tian M-W, Rostami S, Aghakhani S, Goldanlou AS, Qi C. A techno-economic investigation of 2D and 3D configurations of fins and their effects on heat sink efficiency of MHD hybrid nanofluid with slip and non-slip flow. Int J Mech Sci 2021;189:105975.
[14] Gomari SR, Alizadeh R, Alizadeh A, Karimi N. Generation of entropy during forced convection of heat in nanofluid stagnation-point flows over a cylinder embedded in porous media. Numerical Heat Transfer, Part A: Applications 2019;75(10):647–73.
[15] Saeed A, Karimi N, Paul MC. Analysis of the unsteady thermal response of a Li-ion battery pack to dynamic loads. Energy 2021;231:120947.
[16] Keshtegar B, Nehdi ML. Machine learning model for dynamical response of nano-composite pipe conveying fluid under seismic loading. International Journal of Hydromechatronics 2020;3(1):38. https://doi.org/10.1504/IJHM.2020.105499.
[17] Ahmadi MH, Ghazvini M, Sadeghzadeh M, Alhuyi Nazari M, Ghalandari M. Utilization of hybrid nanofluids in solar energy applications: A review. Nano-Structures & Nano-Objects 2019;20:100386. https://doi.org/10.1016/j.nanoso.2019.100386.
[18] Ahmadi MH, Ghazvini M, Sadeghzadeh M, Alhuyi Nazari M, Kumar R, Naeimi A, et al. Solar power technology for electricity generation. A critical review 2018;6(5):340–61.
[19] Wang M, Jiang C, Zhang S, Song X, Tang Y, Cheng H-M. Reversible calcium alloying enables a practical room-temperature rechargeable calcium-ion battery with a high discharge voltage. Nat Chem 2018;10(6):667–72.
[20] Mustafa J, Alqaed S, Kalbasi R. Challenging of using CuO nanoparticles in a flat plate solar collector- Energy saving in a solar-assisted hot process stream. J Taiwan Inst Chem Eng 2021;124:258–65.

[21] Gholipour S, Afrand M, Kalbasi R. Improving the efficiency of vacuum tube collectors using new absorbent tubes arrangement: Introducing helical coil and spiral tube adsorbent tubes. Renewable Energy 2020;151:772–81.
[22] Fudholi A, Sopian K. A review of solar air flat plate collector for drying application. Renew Sustain Energy Rev 2019;102:333–45.
[23] Evangelisti L, De Lieto Vollaro R, Asdrubali F. Latest advances on solar thermal collectors: A comprehensive review. Renew Sustain Energy Rev 2019;114:109318. https://doi.org/10.1016/j.rser.2019.109318.
[24] Borode A, Ahmed N, Olubambi P. A review of solar collectors using carbon-based nanofluids. J Cleaner Prod 2019;241:118311.
[25] Shafieian A, Khiadani M, Nosrati A. A review of latest developments, progress, and applications of heat pipe solar collectors. Renew Sustain Energy Rev 2018;95:273–304.
[26] Pandey KM, Chaurasiya R. A review on analysis and development of solar flat plate collector. Renew Sustain Energy Rev 2017;67:641–50.
[27] Bretado de los Rios MS, Rivera-Solorio CI, García-Cuéllar AJ. Thermal performance of a parabolic trough linear collector using Al2O3/H2O nanofluids. Renewable Energy 2018;122:665–73.
[28] Jebasingh VK, Herbert GMJ. A review of solar parabolic trough collector. Renew Sustain Energy Rev 2016;54:1085–91.
[29] Khan MS, Abid M, Ali HM, Amber KP, Bashir MA, Javed S. Comparative performance assessment of solar dish assisted s-CO2 Brayton cycle using nanofluids. Appl Therm Eng 2019;148:295–306.
[30] Allouhi A, Amine MB, Saidur R, Kousksou T, Jamil A. Energy and exergy analyses of a parabolic trough collector operated with nanofluids for medium and high temperature applications. Energy Convers Manage 2018;155:201–17.
[31] Karimipour A, Bahrami D, Kalbasi R, Marjani A. Diminishing vortex intensity and improving heat transfer by applying magnetic field on an injectable slip microchannel containing FMWNT/water nanofluid. J Therm Anal Calorim 2021;144:2235–46.
[32] Rostami S, Kalbasi R, Talebkeikhah M, Goldanlou AS. Improving the thermal conductivity of ethylene glycol by addition of hybrid nano-materials containing multi-walled carbon nanotubes and titanium dioxide: applicable for cooling and heating. J Therm Anal Calorim 2021;143:1701–12.
[33] Wei H, Afrand M, Kalbasi R, Ali HM, Heidarshenas B, Rostami S. The effect of tungsten trioxide nanoparticles on the thermal conductivity of ethylene glycol under different sonication durations: An experimental examination. Powder Technol 2020;374:462–9.
[34] Govone L, Torabi M, Wang L, Karimi N. Effects of nanofluid and radiative heat transfer on the double-diffusive forced convection in microreactors. J Therm Anal Calorim 2019;135:45–59.
[35] Mu S, Liu Q, Kidkhunthod P, Zhou X, Wang W, Tang Y. Molecular grafting towards high-fraction active nanodots implanted in N-doped carbon for sodium dual-ion batteries. Natl Sci Rev 2020.
[36] Zhang X, Tang Y, Zhang F, Lee C-S. A novel aluminum–graphite dual-ion battery. Adv Energy Mater 2016;6(11):1502588. https://doi.org/10.1002/aenm.201502588.
[37] Tee KF. The influence of water on frequency response of concrete plates armed by nanoparticles utilising analytical approach. International Journal of Hydromechatronics 2020;3(1):51. https://doi.org/10.1504/IJHM.2020.105497.
[38] Bahrami D, Abbasian-Naghneh S, Karimipour A, Karimipour A. Efficacy of injectable rib height on the heat transfer and entropy generation in the microchannel by affecting slip flow. Mathematical Methods in the Applied Sciences 2020.
[39] Nguyen Q, Bahrami D, Kalbasi R, Bach QV. Nanofluid flow through microchannel with a triangular corrugated wall: Heat transfer enhancement against entropy generation intensification. Mathematical Methods in the Applied Sciences 2020.
[40] A. Mwesigye, T. Bello-Ochende, J.P. Meyer, Heat transfer enhancement in a parabolic trough receiver using wall detached twisted tape inserts, in: ASME International Mechanical Engineering Congress and Exposition, Vol. 56291, American Society of Mechanical Engineers, 2013, pp. V06BT07A031.
[41] Ghadirijafarbeigloo S, Zamzamian A, Yaghoubi M. 3-D numerical simulation of heat transfer and turbulent flow in a receiver tube of solar parabolic trough concentrator with louvered twisted-tape inserts. Energy Procedia 2014;49:373–80.
[42] Song X, Dong G, Gao F, Diao X, Zheng L, Zhou F. A numerical study of parabolic trough receiver with nonuniform heat flux and helical screw-tape inserts. Energy 2014;77:771–82.
[43] Chang C, Xu C, Wu Z, Li X, Zhang Q, Wang Z. Heat transfer enhancement and performance of solar thermal absorber tubes with circumferentially non-uniform heat flux. Energy Procedia 2015;69:320–7.
[44] Mwesigye A, Bello-Ochende T, Meyer JP. Heat transfer and entropy generation in a parabolic trough receiver with wall-detached twisted tape inserts. Int J Therm Sci 2016;99:238–57.
[45] Liu Y, Chen Q, Hu K, Hao J-H. Flow field optimization for the solar parabolic trough receivers in direct steam generation systems by the variational principle. Int J Heat Mass Transf 2016;102:1073–81.
[46] Jaramillo O, Borunda M, Velazquez-Lucho K, Robles M. Parabolic trough solar collector for low enthalpy processes: An analysis of the efficiency enhancement by using twisted tape inserts. Renewable Energy 2016;93:125–41.
[47] Zhu X, Zhu L, Zhao J. Wavy-tape insert designed for managing highly concentrated solar energy on absorber tube of parabolic trough receiver. Energy 2017;141:1146–55.
[48] Rawani A. enhancement in thermal performance of parabolic trough collector with serrated twisted tape inserts. Int J Thermodyn 2017;20:111–9.
[49] Liu P, Zheng N, Liu Z, Liu W. Thermal-hydraulic performance and entropy generation analysis of a parabolic trough receiver with conical strip inserts. Energy Convers Manage 2019;179:30–45.
[50] Amani K, Ebrahimpour M, Akbarzadeh S, Valipour MS. The utilization of conical strip inserts in a parabolic trough collector. J Therm Anal Calorim 2020;140(3):1625–31.
[51] Suresh Isravel R, Raja M, Saravanan S, Vijayan V. Thermal augmentation in parabolic trough collector solar water heater using rings attached twisted tapes. Mater Today: Proc 2020;21:127–9.
[52] Ti Z, Deng XW, Zhang M. Artificial Neural Networks based wake model for power prediction of wind farm. Renewable Energy 2021;172:618–31.
[53] Vasanthi P, Reddy G. Experimental investigations on heat transfer and friction factor of hybrid nanofliud equiped with angular twisted strip inserts in a parabolic trough solar collector under turbulent flow. Int. J. Innov. Sci. Eng. Technol 2021;8:1.
[54] Diwan K, S. Soni M. Heat transfer enhancement in absorber tube of parabolic trough concentrators using wire-coils inserts, Universal Journal of. Mechanical Engineering 2015;3(3):107–12.
[55] Şahin HM, Baysal E, Dal AR, Şahin N. Investigation of heat transfer enhancement in a new type heat exchanger using solar parabolic trough systems. Int J Hydrogen Energy 2015;40(44):15254–66.
[56] Yılmaz İH, Mwesigye A, Göksu TT. Enhancing the overall thermal performance of a large aperture parabolic trough solar collector using wire coil inserts. Sustainable Energy Technol Assess 2020;39:100696.
[57] Afrand M. Using a magnetic field to reduce natural convection in a vertical cylindrical annulus. Int J Therm Sci 2017;118:12–23.
[58] Afrand M, Farahat S, Nezhad AH, Ali Sheikhzadeh G, Sarhaddi F. 3-D numerical investigation of natural convection in a tilted cylindrical annulus containing molten potassium and controlling it using various magnetic fields. Int J Appl Electromagnet Mech 2014;46:809–21.
[59] Afrand M, Farahat S, Nezhad AH, Sheikhzadeh GA, Sarhaddi F. Numerical simulation of electrically conducting fluid flow and free convective heat transfer in an annulus on applying a magnetic field. Heat Transfer Research 2014;45(8):749–66.
[60] Afrand M, Farahat S, Nezhad AH, Sheikhzadeh GA, Sarhaddi F, Wongwises S. Multi-objective optimization of natural convection in a cylindrical annulus mold under magnetic field using particle swarm algorithm. Int Commun Heat Mass Transfer 2015;60:13–20.
[61] Kalbasi R. Introducing a novel heat sink comprising PCM and air – Adapted to electronic device thermal management. Int J Heat Mass Transf 2021;169:120914.
[62] Alizadeh R, Karimi N, Mehdizadeh A, Nourbakhsh A. Analysis of transport from cylindrical surfaces subject to catalytic reactions and non-uniform impinging flows in porous media. J Therm Anal Calorim 2019;138:659–78.
[63] Torabi M, Karimi N, Zhang K, Peterson G. Generation of entropy and forced convection of heat in a conduit partially filled with porous media–local thermal non-equilibrium and exothermicity effects. Appl Therm Eng 2016;106:518–36.
[64] Giwa SO, Sharifpur M, Ahmadi MH, Meyer JP. Magnetohydrodynamic convection behaviours of nanofluids in non-square enclosures: A comprehensive review. Mathematical Methods in the Applied Sciences 2020.
[65] Giwa SO, Sharifpur M, Ahmadi MH, Meyer JP. A review of magnetic field influence on natural convection heat transfer performance of nanofluids in square cavities. J Therm Anal Calorim 2021;145(5):2581–623.
[66] Mahdavi M, Garbadeen I, Sharifpur M, Ahmadi MH, Meyer JP. Study of particle migration and deposition in mixed convective pipe flow of nanofluids at different inclination angles. J Therm Anal Calorim 2019;135:1563–75.
[67] Mahdavi M, Sharifpur M, Ahmadi MH, Meyer JP. Aggregation study of Brownian nanoparticles in convective phenomena. J Therm Anal Calorim 2019;135:111–21.
[68] Nwosu PN, Meyer J, Sharifpur M. Nanofluid Viscosity: A simple model selection algorithm and parametric evaluation. Comput Fluids 2014;101:241–9.
[69] Cheng L, Zhu Y, Band SS, Bahrami D, Kalbasi R, Karimipour A, et al. Role of gradients and vortexes on suitable location of discrete heat sources on a sinusoidal-wall microchannel. Engineering Applications of Computational Fluid Mechanics 2021;15:1176–90.
[70] Bahrami D, Nadooshan AA, Bayareh M. Numerical study on the effect of planar normal and Halbach magnet arrays on micromixing. Int J Chem Reactor Eng 2020;18.